Simulation of the ASTRI demonstration particle receiver during on-sun testing

Daniel Potter[1], Jin-Soo Kim[1], Sahan Kuruneru[1], and Geoff Drewer[1]

[1]CSIRO Energy Centre, 10 Murray Dwyer Cct, Mayfield West NSW 2304 Australia
daniel.potter@csiro.au

Heliostat field optics and receiver heat transfer simulations were performed for the ASTRI demonstration particle receiver under measured experimental conditions during the on-sun test campaign at CSIRO Newcastle. The on-sun test of the particle receiver system commenced in December 2021, and present work considers experiments performed between May 2022 and March 2023 where the receiver was operated in a "continuous heating" mode that allowed outlet temperatures up to 700°C and thermal outputs up to 600kW to be reached. Whilst reasonable agreement is observed between measurement and simulation for the timeseries trend of receiver outlet temperature, discrepancies are found for receiver thermal output and efficiency, especially at elevated (above 400°C) inlet temperatures where thermal expansion effects are significant.

Receiver design and operation

The ASTRI demonstration particle receiver implements a novel multi-stage falling particle curtain concept with a truncated cone geometry and is designed for a nominal thermal capacity of 750kWt with particle inlet and outlet temperatures of 600 and 800°C respectively (Kim et al., 2020). The particle curtain is located within a cavity with an 800mm diameter aperture tilted down 45° from the horizon. The particle flow rate is controlled by a slide gate that allows particles to flow in from a hopper above the receiver. The particle mass flow rate is determined by measuring the hopper mass with a load cell at regular time intervals. The particle temperature at various points of interest in the system is measured with thermocouples, including at the receiver inlet and outlet. Although the particle system installed at CSIRO Newcastle includes a heat exchanger for cooling the heated particles, the experiments considered in the present work (performed between May 2022 and March 2023) involved the receiver being operated in a "continuous heating" mode where the heated particles from the receiver outlet were conveyed directly back up to the receiver inlet without being passed through the heat exchanger. By operating in this manner, the receiver inlet and outlet temperatures were slowly increased over operating windows of approximately 1 to 2 hours duration, reaching outlet temperatures of up to 700°C and thermal outputs up to 600kW. Along with the particle mass flow rate and temperature measurements, the DNI, heliostat field utilisation and heliostat calibration images are also recorded during the experiments. Using this information, the particle receiver performance can be simulated with a numerical model and comparisons made with the experimental measurements.

Physical modelling

Computational tools from the Heliosim software family (Potter, 2022) were used to perform heliostat field optics and receiver heat transfer simulations. The receiver components relevant to optics and heat transfer modelling (i.e. casing, aperture shielding, insulation, deflector plate, and particle curtain) are described by a collection of surface meshes, Figure 1. The surface meshes for the front and rear sides of the particle curtain are carefully created so that a collection of particle flow "channels" can be easily defined by the columns of triangular facet pairs. A quasi-steady state energy balance is formulated for each mesh facet, and a surface temperature for each mesh facet is calculated by solving the set of nonlinear equations. Concentrated solar radiation from the solar field and thermal radiation inside the cavity are modelled using Monte Carlo ray tracing. Convective losses are approximated using surface-specific heat transfer coefficient correlations (e.g. Figure 2 for the particle curtain and back wall surfaces) derived from coarse-grained CFD-DPM simulations using OpenFOAM (Kuruneru et al., 2022). One dimensional conduction heat transfer is considered between the insulation and casing facets where the thermal conductivity of the insulation is assumed constant through its thickness. For the facets describing the approximate location of the

particle curtain front and rear surfaces, the advection of thermal energy along each of the "channels" by the particle motion is also considered in the energy balance. The particle curtain is treated in an approximate manner where 1) mixing between adjacent channels is assumed to be negligible, 2) constant temperature is assumed through the curtain thickness, and 3) optical properties are calculated using correlations (Kim et al., 2019). Curtain absorptance, reflectance and transmittance for a particle mass flow rate of 2.73kg/s are displayed in Figure 3, with the locations of the inlet, troughs and outlets indicated.

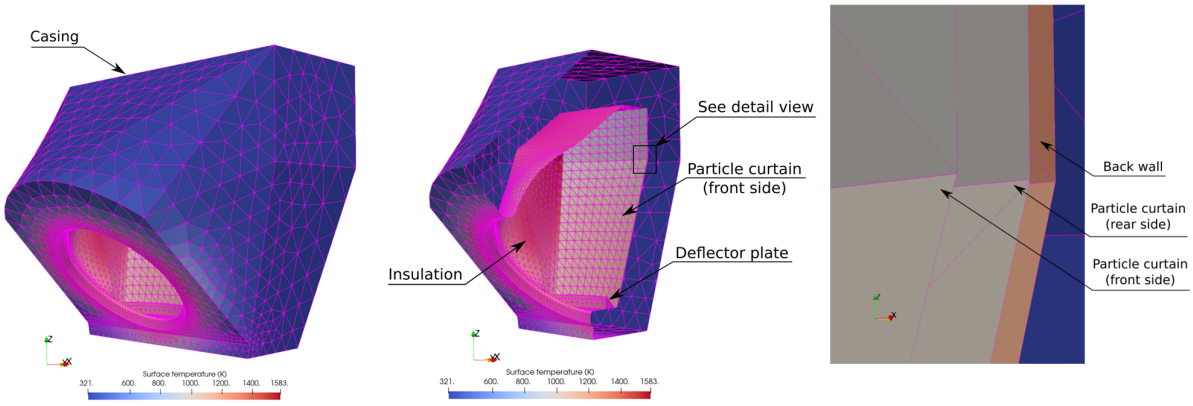

Figure 1. Particle receiver surface mesh for optics and heat transfer simulations

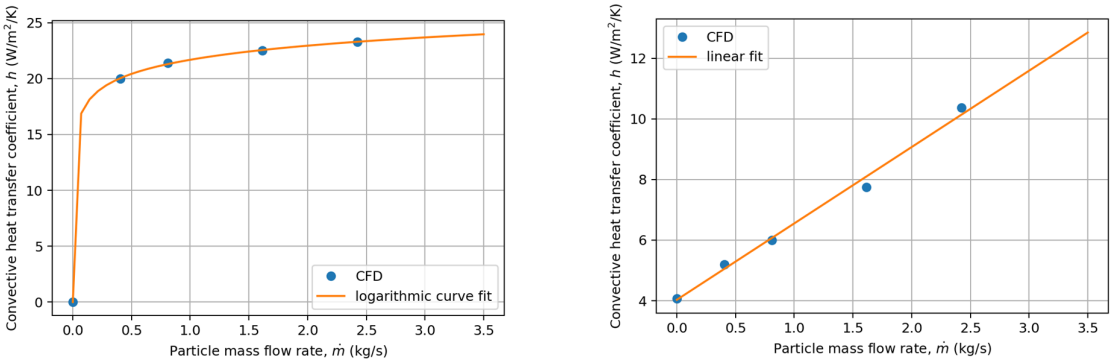

(a) Particle curtain (using single-sided area) (b) Back wall

Figure 2. Convective heat transfer coefficients derived from CFD-DPM simulations

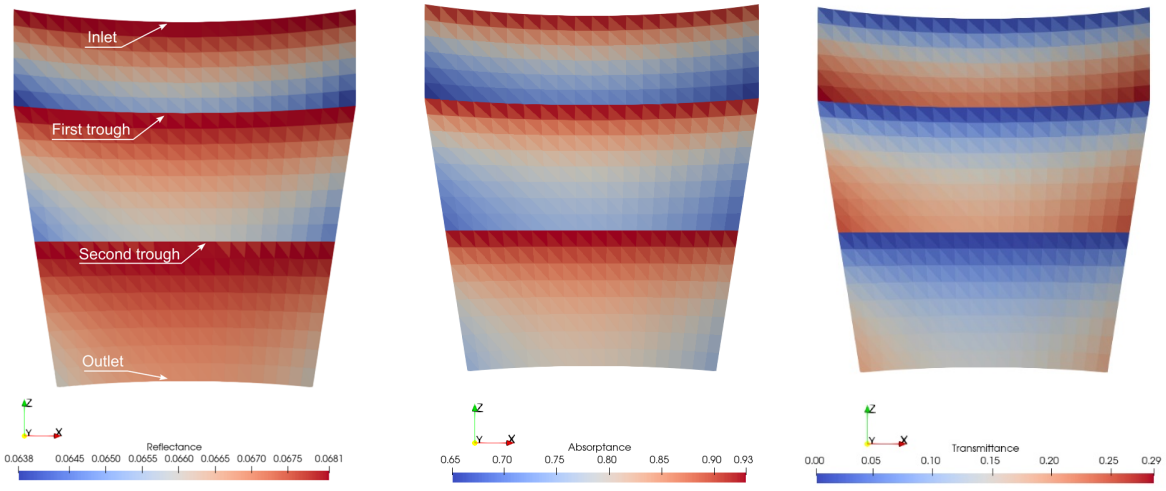

Figure 3. Curtain optical properties for a particle mass flow rate of 2.73kg/s

Results

Four days of on-sun testing were selected for simulation. The particle inlet and outlet temperatures, particle mass flow rate, ambient temperature, DNI, heliostat tracking error (1.5mrad in each heliostat rotation axis) and heliostat field utilisation information were extracted from the experiment measurements. Values for heliostat slope error (1.4mrad), heliostat reflectance (0.9) and circumsolar ratio (0.02) were assumed based on prior analyses. A comparison between the measured and simulated particle outlet temperature timeseries are presented in Figure 4.

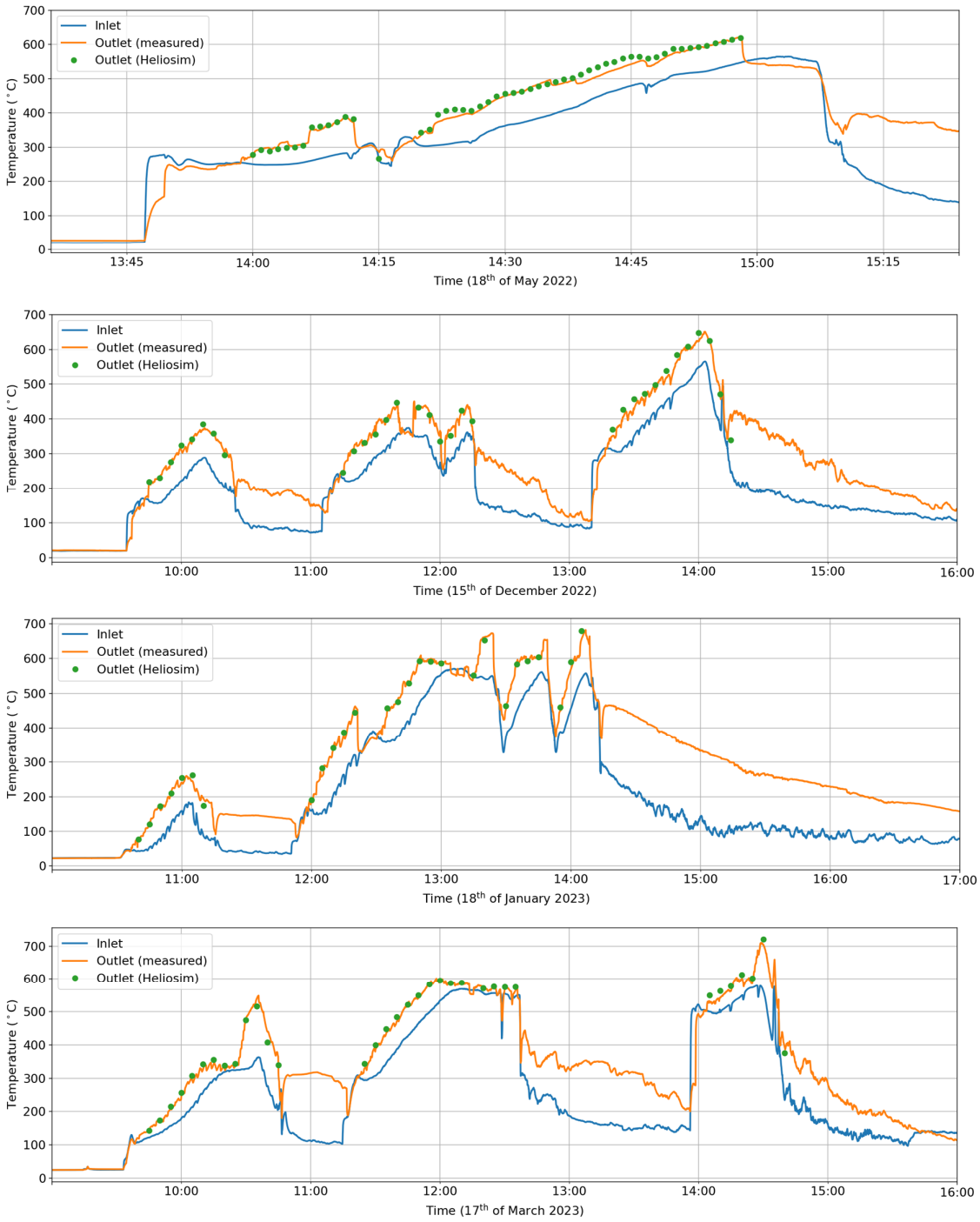

Figure 4. Comparison of measured and simulated receiver outlet temperatures

The measured and simulated results from the four days of operation were then aggregated and analysed, Figure 5. A degree of correlation between average error in thermal output and inlet temperature is observed, Figure 5a, with the largest errors occurring at inlet temperatures above 400°C. This is possibly due to inaccuracies in the mass flow rate measurement at high temperature. Inspection after high temperature operation indicated that thermal expansion was preventing the load cell from being exposed to the full hopper weight. Measured and simulated receiver efficiency are plotted as a function of receiver thermal output in Figure 5b. The receiver efficiency is computed as the thermal power output captured by the particles divided by the solar radiation flux through the aperture. For the measured receiver efficiency, aperture flux is not known, and the simulated value is used. The simulated receiver efficiency is observed to peak at almost 90%, and to be consistently above 80% at the higher power levels. The measured receiver efficiency is observed to have larger spread and even exceed unity in some instances. Errors in the measured mass flow rate, measured temperatures and simulated aperture flux are being investigated as possible causes of the higher than unity measured efficiency values.

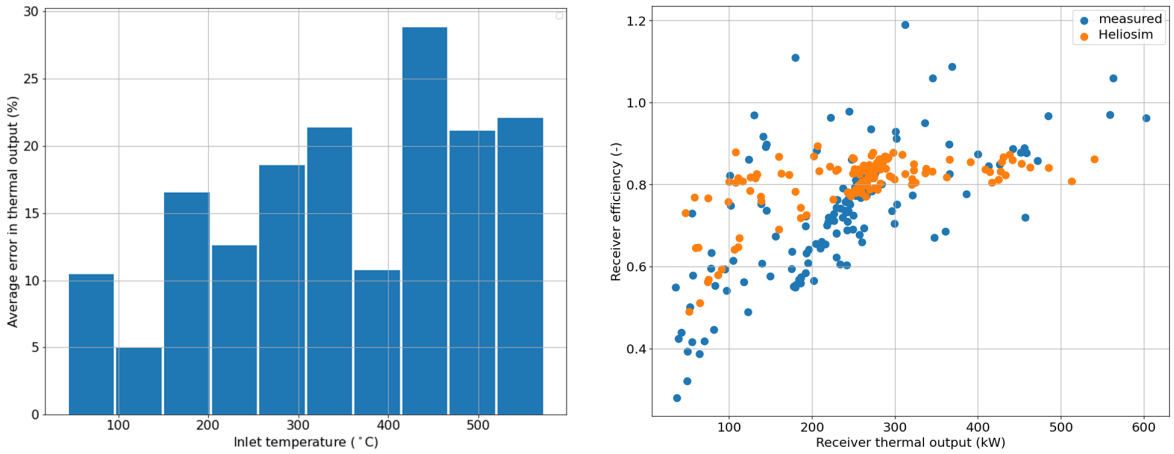

(a) Histogram of error in thermal output

(b) Receiver efficiency versus thermal output

Figure 5. Aggregated analysis of measured and simulated receiver performance

Conclusion

Whilst reasonable agreement is observed between measurement and simulation for the timeseries trend of receiver outlet temperature, significant discrepancy is found for receiver thermal output and receiver efficiency, especially at elevated (above 400°C) inlet temperatures where thermal expansion effects are known to have caused errors in the mass flow rate measurements. The ASTRI demonstration particle receiver on-sun testing campaign is ongoing, and improved mass flow rate and heliostat optical error measurement techniques are being implemented.

References

Kim, J.-S., Gardner, W., Potter, D., & Soo Too, Y. C. (2020). 'Design of a multi-stage falling particle receiver with truncated-cone geometry'. *AIP Conference Proceedings*, 2303.

Kim, J.-S., Kumar, A., Gardner, W., & Lipiński, W. (2019). 'Numerical and experimental investigation of a novel multi-stage falling particle receiver'. *AIP Conference Proceedings*, 2126.

Kuruneru, S. T. W., Kim, J.-S., Soo Too, Y. C., & Potter, D. (2022). 'Discrete particle modelling of buoyant convective particle-laden air flow in solar cavity free-falling particle receivers'. *Energy Reports*, 8, p3902–3918.

Potter, D. (2022). 'The Heliosim software family: modelling, design, and control tools for CST systems'. *Proceedings of the Asia Pacific Solar Research Conference 2022*.